



HAL
open science

Implicit Implementation of Nonsmooth Controllers to Nonsmooth Actuators

Ryo Kikuuwe, Yuki Yamamoto, Bernard Brogliato

► **To cite this version:**

Ryo Kikuuwe, Yuki Yamamoto, Bernard Brogliato. Implicit Implementation of Nonsmooth Controllers to Nonsmooth Actuators. *IEEE Transactions on Automatic Control*, 2022, 67 (9), pp.4645-4657. 10.1109/TAC.2022.3163124 . hal-03180790v2

HAL Id: hal-03180790

<https://inria.hal.science/hal-03180790v2>

Submitted on 4 Feb 2022

HAL is a multi-disciplinary open access archive for the deposit and dissemination of scientific research documents, whether they are published or not. The documents may come from teaching and research institutions in France or abroad, or from public or private research centers.

L'archive ouverte pluridisciplinaire **HAL**, est destinée au dépôt et à la diffusion de documents scientifiques de niveau recherche, publiés ou non, émanant des établissements d'enseignement et de recherche français ou étrangers, des laboratoires publics ou privés.

Implicit Implementation of Nonsmooth Controllers to Nonsmooth Actuators

Ryo Kikuuwe^{*†}, Yuki Yamamoto^{*}, and Bernard Brogliato[‡]

February 4, 2022, 10:25

Abstract

This paper presents an approach to implement a sliding-mode position controller to a plant equipped with a nonsmooth actuator. The actuator is modeled as a set-valued function from the control input and the velocity to the actuator force, which is motivated by quasistatic characteristics of hydraulic actuators shown in a previous study. The implementation of the sliding-mode controller is performed with the implicit discretization of the nominal plant model and the controller, which copes with the difficulties caused by set-valuedness, such as numerical chattering. Stability analyses both in the continuous-time and discrete-time domains are presented. Simulation results illustrate the theoretical findings.

Keywords: hydraulic actuators, sliding-mode control, set-valuedness, differential inclusions, implicit discretization

1 Introduction

Recently Kikuuwe et al. [16] presented a quasistatic modeling approach for hydraulic actuators used in commercial excavators. The actuator model presented in [16] is described as a nonsmooth function from the velocity to the force that depends on the valve openings. The actuator force is set-valued at the zero velocity because the closed valves prevent the oil flow as well as the motion of the piston, and the actuator force is subject to velocity-dependent limits because of the relief valves and the pressure drop at the control valves. This quasistatic actuator model has a form that is quite unfamiliar to the control community, and thus poses a new, interesting class of control problems. Such problems would be worth tackling not only for hydraulic actuators but also for yet-unknown future actuators.

This paper deals with the position control problem of a second-order plant driven by a nonsmooth actuator of a class that includes Kikuuwe et al.'s [16] quasistatic model of hydraulic actuators. The whole control system discussed in this paper is illustrated in

^{*}Graduate School of Advanced Science and Engineering, Hiroshima University, 1-4-1 Kagamiyama, Higashi-Hiroshima, Hiroshima 739-8527, Japan.

[‡]Univ. Grenoble-Alpes, INRIA, CNRS, Grenoble INP, LJK, 38000 Grenoble, France.

[§]Corresponding Author. e-mail: kikuuwe@ieee.org

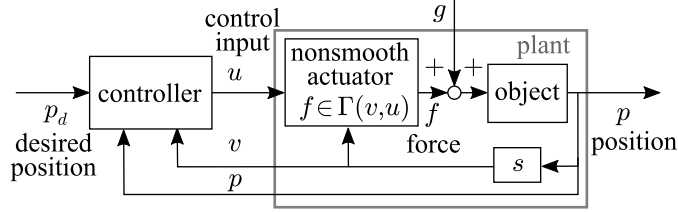


Figure 1: Position control problem discussed in this paper.

Fig. 1. The actuator is assumed to be set-valued and subject to velocity-dependent saturation. We consider implementing a sliding-mode controller for the convenience of dealing with the saturation and also of designing the convergent behavior to the target position [14,15,19]. Practically speaking, this problem setting is important for semi-automatic or remote-controlled hydraulic excavators that may receive target position commands set far from the current position. It cannot be easily handled by many of the existing techniques, which are based on simple proportional-integral (PI) control [24, 25, 28, 33, 34] or linearized actuator models [20, 30] neglecting the actuator saturation brought about by the relief valves. This paper intends to prepare theoretical foundations for this problem without restricting its scope to hydraulic systems.

In the use of actuators of particular characteristics, one of the common approaches is to use the inverse models of the actuator models, which map the control input to the actuator force. This approach has been employed mainly for actuators with hysteresis [4,9,10]. Previous studies have investigated applications to piezoactuators [9], magnetostrictive actuators [4], shape memory alloys [4], reluctance motors [31], and electro-hydraulic systems [21]. Other types of nonlinearity, such as dead-zone and backlash [10] and creep [9], have also been considered. The application of such an approach to our problem is not straightforward because of the set-valuedness of the actuator model, which makes the whole plant dynamics governed by a differential inclusion. Moreover, using sliding-mode control injects another set-valuedness into the closed-loop system, posing additional difficulty.

The mathematical treatment of nonsmooth dynamical systems involving the set-valuedness has been investigated by some researchers. For simulation purposes, implicit discretization has been known to be useful for a long time [1, 2, 18]. With the implicit discretization, the set-valuedness, such as Coulomb friction, rigid-body contact, and an ideal sliding-mode controller, is enclosed within an *algebraic loop*, which is an algebraic constraint between the input and the output and can be seen as a feedback loop without latency. At every timestep, the algebraic constraints are solved either analytically or numerically. This scheme has also been employed for control purposes, specifically, for the implementation of nonsmooth controllers, of which the outputs are set-valued [3, 7, 11–13, 22, 23, 27]. In the implicit implementation scheme, an algebraic loop is formed between a nominal plant model and the nonsmooth controller, and the solution of the algebraic constraint is used as the control input at every sampling step. In other words, this implementation scheme employs a one-step state predictor based on the nominal plant model.

This paper presents an approach to implement nonsmooth controllers to plants equipped

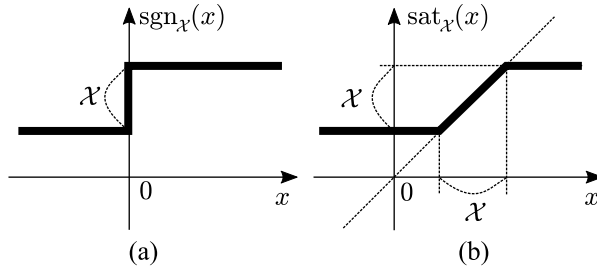


Figure 2: Graphs of $\text{sgn}_{\mathcal{X}}(x)$ and $\text{sat}_{\mathcal{X}}(x)$.

with intrinsically nonsmooth actuators. The actuator force to be generated is determined by a one-step predictor based on the nominal model of the plant. The determined force is converted into the control input through the inverse map of the quasistatic actuator model using the predicted velocity obtained by the nominal plant model. Some theoretical analysis and illustrative simulation results are presented.

The remainder of this paper is organized as follows. Section 2 introduces some preliminaries. Section 3 shows problem settings including the details of the nonsmooth plant model. Section 4 proposes a simple sliding-mode controller and its discrete-time implementation to the nonsmooth plant. Section 5 shows some illustrative simulation results. Section 6 provides concluding remarks.

2 Mathematical Preliminaries

In this paper, \mathbb{R} denotes the set of all real numbers, \mathbb{R}_+ denotes the set of all non-negative real numbers, \mathbb{N} denotes the set of all non-negative integers, and \mathcal{B} denotes the unit closed ball in \mathbb{R} , i.e., $\mathcal{B} \triangleq [-1, 1] \subset \mathbb{R}$, which is in fact a closed interval. For a set \mathcal{Z} , $\text{conv}\mathcal{Z}$ stands for the convex hull of \mathcal{Z} . It should be recalled that a closed and bounded interval in \mathbb{R} means a compact convex subset of \mathbb{R} . The notation $f : \mathcal{X}_0 \rightarrow \mathcal{X}_1$ means that f is a single-valued function from the set \mathcal{X}_0 to the set \mathcal{X}_1 , and $f : \mathcal{X}_0 \rightrightarrows \mathcal{X}_1$ means that f is a set-valued function from the set \mathcal{X}_0 to the set \mathcal{X}_1 . The notation $\mathcal{X}_0 \times \mathcal{X}_1$ stands for the direct product of the sets \mathcal{X}_0 and \mathcal{X}_1 .

This paper uses the following functions:

$$\text{sgn}_{\mathcal{X}}(x) \triangleq \begin{cases} \min \mathcal{X} & \text{if } x < 0 \\ \mathcal{X} & \text{if } x = 0 \\ \max \mathcal{X} & \text{if } x > 0 \end{cases} \quad (1)$$

$$\text{sat}_{\mathcal{X}}(x) \triangleq \begin{cases} \min \mathcal{X} & \text{if } x < \min \mathcal{X} \\ x & \text{if } x \in \mathcal{X} \\ \max \mathcal{X} & \text{if } x > \max \mathcal{X} \end{cases} \quad (2)$$

where \mathcal{X} is a closed and bounded interval in \mathbb{R} . These functions are illustrated in Fig. 2. For brevity, we write

$$\text{sgn}(x) \triangleq \text{sgn}_{\mathcal{B}}(x), \quad \text{sat}(x) \triangleq \text{sat}_{\mathcal{B}}(x). \quad (3)$$

The functions have the following properties:

Lemma 1. Let \mathcal{X} be a closed and bounded interval in \mathbb{R} and $x, y \in \mathbb{R}$ be real numbers. Then, the following statement holds true:

$$y \in \text{sgn}_{\mathcal{X}}(x - y) \iff y = \text{sat}_{\mathcal{X}}(x). \quad (4)$$

Proof. Let $[A, B] \triangleq \mathcal{X}$. Then, $y \in \text{sgn}_{\mathcal{X}}(x - y) \iff (y = A \wedge x - y < 0) \vee (y \in \mathcal{X} \wedge x - y = 0) \vee (y = B \wedge x - y > 0) \iff (y = A \wedge x < A) \vee (y = x \wedge x \in \mathcal{X}) \vee (y = B \wedge x > B) \iff y = \text{sat}_{\mathcal{X}}(x)$. \square

Lemma 2. Let \mathcal{X} be a closed and bounded interval in \mathbb{R} and let $a > 0$ and $b, x \in \mathbb{R}$ be real numbers. Then, the following statement holds true:

$$x = \text{sat}_{\mathcal{X}}(b - ax) \iff x = \text{sat}_{\mathcal{X}}(b/(a + 1)). \quad (5)$$

Proof. Let $[A, B] = \mathcal{X}$. Then, $x = \text{sat}_{\mathcal{X}}(b - ax) \iff (b - ax < A \wedge x = A) \vee (x = b - ax \wedge x \in \mathcal{X}) \vee (b - ax > B \wedge x = B) \iff (x = A \wedge b/(a + 1) < A) \vee (x = b/(1 + a) \wedge b/(a + 1) \in \mathcal{X}) \vee (x = B \wedge b/(a + 1) < B) \iff x = \text{sat}_{\mathcal{X}}(b/(a + 1))$. \square

It should be noted that these proof can be greatly simplified by using the tools of convex analysis, such as normal cones. For example, Lemma 1 can be simply proven as $y \in \text{sgn}_{\mathcal{X}}(x - y) \iff x - y \in N_{\mathcal{X}}(y) \iff y = \text{proj}(\mathcal{X}; x) = \text{sat}_{\mathcal{X}}(x)$. (See Appendix B of [6] for definitions and see Proposition 6.47 of [5] for a detailed proof.)

This paper uses the inequality signs ($<$, $>$, \leq and \geq) with the subscript \forall to write inequalities involving sets, which should be read as follows:

$$x <_{\forall} \mathcal{Y} \iff (x < y, \forall y \in \mathcal{Y}) \quad (6)$$

$$\mathcal{X} <_{\forall} y \iff (x < y, \forall x \in \mathcal{X}) \quad (7)$$

$$\mathcal{X} <_{\forall} \mathcal{Y} \iff (x < y, \forall x \in \mathcal{X}, \forall y \in \mathcal{Y}) \quad (8)$$

where \mathcal{X} and \mathcal{Y} are sets of real numbers.

A set-valued function Φ is said to be monotone if $(\Phi(x_1) - \Phi(x_2))(x_1 - x_2) \forall \geq 0$ for all x_1 and x_2 . It is said to be strictly monotone if $(\Phi(x_1) - \Phi(x_2))(x_1 - x_2) \forall > 0$ for all x_1 and x_2 satisfying $x_1 \neq x_2$. A set-valued function Φ maps a set \mathcal{Z} in the following manner:

$$\Phi(\mathcal{Z}) = \bigcup_{x \in \mathcal{Z}} \Phi(x). \quad (9)$$

As a consequence of (9), expressions involving nested set-valued functions (i.e., compositions of set-valued functions) should be read as follows:

$$\Phi_1(\Phi_2(x)) = \bigcup_{y \in \Phi_2(x)} \Phi_1(y), \quad (10)$$

as is the case also in [22].

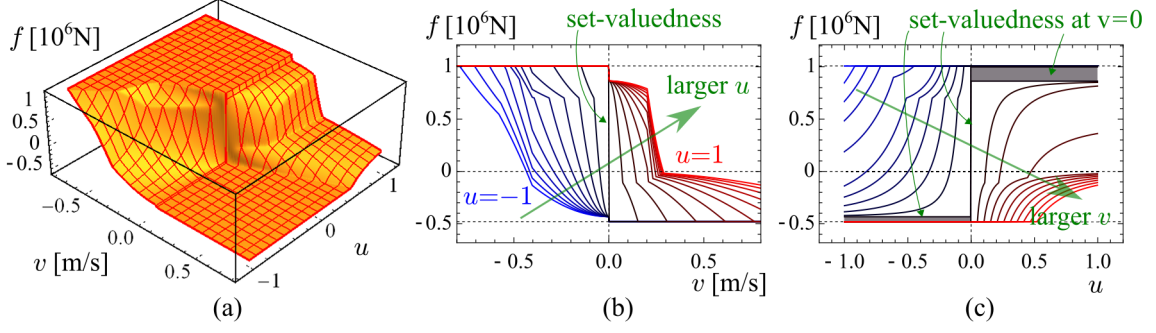


Figure 3: Graph of $\Gamma(v, u)$ presented in [16]. It is set-valued at $v = 0$.

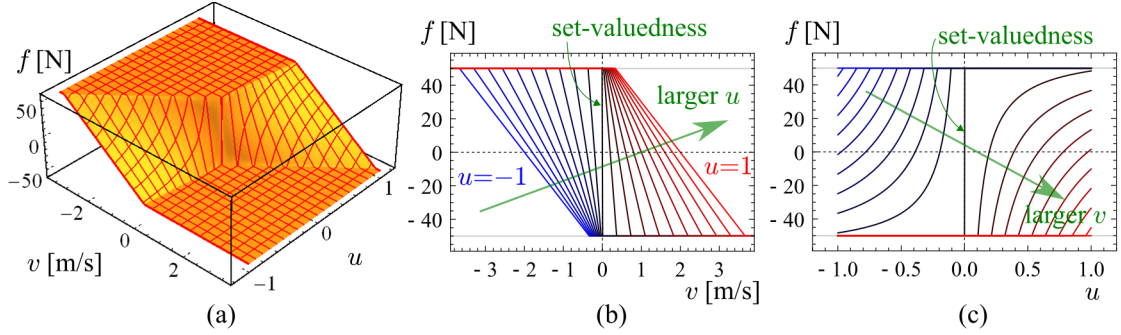


Figure 4: Graph of $\Gamma_{\text{ex}}(v, u)$ defined in (11) with $\{F, F_m, B\} = \{50 \text{ N}, 60 \text{ N}, 30 \text{ Ns/m}\}$. It is set-valued at $\{v, u\} = \{0, 0\}$.

3 Nonsmooth Actuator

3.1 Actuator and Plant

Now, let \mathcal{F} be a closed and bounded interval in \mathbb{R} including zero in its interior, i.e., $\mathcal{F} = [\min \mathcal{F}, \max \mathcal{F}]$ and $\min \mathcal{F} < 0 < \max \mathcal{F}$. The core of the problem discussed in this paper is a class of set-valued functions $\Gamma : \mathbb{R} \times \mathcal{B} \rightrightarrows \mathcal{F}$ that possess the following properties:

- P1** For all $v \in \mathbb{R}$ and $u \in \mathcal{B}$, $\Gamma(v, u)$ is a closed and bounded interval in \mathbb{R} .
- P2** For all $v \in \mathbb{R}$, $\Gamma(v, \mathcal{B}) = \text{conv}(\Gamma(v, -1) \cup \Gamma(v, 1)) \subseteq \mathcal{F}$, which is a closed and bounded interval in \mathbb{R} .
- P3** Γ is upper semicontinuous [26, p.32] in the set-valued sense.
- P4** For all $u \in \mathcal{B}$, $\Gamma(-v, u)$ is monotone with respect to v .
- P5** For all $v \in \mathbb{R}$, both $\max \Gamma(v, u)$ and $\min \Gamma(v, u)$ are monotone functions of u . (Note that $\Gamma(v, u) = \max \Gamma(v, u) = \min \Gamma(v, u)$ if $\Gamma(v, u)$ is a singleton.)
- P6** $\Gamma(v, 0) = \text{sgn}_{\mathcal{F}}(-v)$ for all $v \in \mathbb{R}$.
- P7** $\Gamma(0, u) \searrow < 0$ for all $u \in [-1, 0)$ and $\Gamma(0, u) \searrow > 0$ for all $u \in (0, 1]$.

From the properties P1 to P7, the following properties are deduced:

PD1 $\Gamma(0, 0) = \mathcal{F}$ (from P6).

PD2 $\Gamma(v, u) = \max \mathcal{F}$ if $v < 0$ and $u > 0$, i.e., in the second quadrant of the v - u plane, and $\Gamma(v, u) = \min \mathcal{F}$ if $v > 0$ and $u < 0$, i.e., in the fourth quadrant of the v - u plane (from P4, P5, P6, and P7).

PD3 The set $\Gamma(v, \mathcal{B})$ coincides with \mathcal{F} when $v = 0$ (from P6), and becomes smaller as $|v|$ increases (from P4).

This paper uses this class of functions Γ as a quasistatic model of an actuator that produces a force satisfying $f \in \Gamma(v, u)$ at the velocity $v \in \mathbb{R}$ according to the dimensionless control input $u \in \mathcal{B}$. It may or may not be set-valued when $\{v, u\} \neq \{0, 0\}$. The actuator force f belongs to the velocity-dependent set $\Gamma(v, \mathcal{B})$. It can be increased by increasing the control input u (due to P5) and by decreasing the velocity v (due to P4), in such a way as if the actuator includes an internal nonlinear viscous resistance. When the control input u is zero, the actuator acts exactly like the Coulomb friction (due to P6), of which the force always opposes the velocity.

One example of Γ is illustrated in Fig. 3, which has been presented in [16]. Another one, which is much simpler, can be given as follows:

$$\Gamma_{\text{ex}}(v, u) \triangleq \begin{cases} \text{sat}_{F\mathcal{B}}(F_m \text{sgn}(u) - Bv/|u|) & \text{if } |u| \in (0, 1] \\ \text{sgn}_{F\mathcal{B}}(-v) & \text{if } u = 0 \end{cases} \quad (11)$$

where $F_m \geq F > 0$ and $B > 0$. This function Γ_{ex} is illustrated in Fig. 4. In Fig. 3(a) and Fig. 4(a), for example, the property P6 is visible as the vertical line at $\{v, u\} = \{0, 0\}$, and the property PD2 is visible as the highest and lowest plateaus.

This paper discusses the position control problem of the plant with the following dynamics:

$$M\dot{v} \stackrel{\text{a.e.}}{=} f + g, \quad \dot{p} = v \quad (12a)$$

$$f \stackrel{\text{a.e.}}{\in} \Gamma(v, u). \quad (12b)$$

Here, ‘‘a.e.’’ stands for ‘‘almost everywhere in time.’’ The plant (12) in combination with a position controller is illustrated in Fig. 1. Here, we refer to (12a) as the controlled object, which consists of a mass $M > 0$ with position $p \in \mathbb{R}$ and velocity $v \in \mathbb{R}$. The mass is subjected to the external force $g \in \mathbb{R}$ and the actuator force $f \in \mathbb{R}$. We assume that g is bounded and is a piecewise-continuous function of time t . The actuator is modeled as Γ in (12b) and it applies the force f to the plant, depending on the plant velocity v and the control input u . The control input u is provided by the controller to be combined with this plant, as illustrated in Fig. 1. Because of the properties P1 and P3, the differential inclusion (12) always has an absolutely continuous solution v if $u \in \mathcal{B}$ is a measurable function of time t . (See, e.g., [26, Theorem 4.7], the three conditions therein being satisfied.)

One important feature of the plant (12) is that, when the external force g is zero, $\dot{v} = 0$ can be established at the velocity v_{ss} satisfying $0 \in \Gamma(v_{ss}, u)$, which means that the steady-state velocity v_{ss} can be manipulated through the control input u . In this

sense, the actuator (12b) can be said to be a force-saturated, weakly-velocity-commanded system. In the special case where $\Gamma = \Gamma_{\text{ex}}$ in (11), we have $v_{ss} = F_m u / B$.

As far as the authors are currently aware, the hydraulic actuator model presented in [16] is the only example that can be represented by the map Γ . Because it is a static map, actuators exhibiting hysteresis, such as piezoactuators, would not fall within this class of actuators.

Remark 1. *The dependence of $\Gamma(v, u)$ on the velocity v is crucial in our problem setting. For example, if Γ is defined as $\Gamma(v, u) = F \text{sgn}(u)$ with $F > 0$ and $u \equiv 0$, the differential inclusion (12) reduces to $M\dot{v} \in [-F, F]$, which does not have a unique solution obviously. According to Theorem 1 in [8], with $\Gamma(v, u)$ possessing the property P4, the differential inclusion (12) has unique solutions from almost all initial values of $v \in \mathbb{R}$.*

3.2 Inverse Model of Actuator

When an actuator is used in a control system, a controller should usually be constructed so that it determines the actuator force to be generated. In order to use such a controller with an actuator of the form of (12b), one needs to convert the desired actuator force \hat{f} to a control input u sent to the actuator using an inverse model of the actuator. For this purpose, we define a set-valued function $\Theta : \mathbb{R} \times \mathcal{F} \rightrightarrows \mathcal{B}$ that satisfies the following:

$$u \in \Theta(v, \hat{f}) \iff \hat{f} \in \Gamma(v, u). \quad (13)$$

It means that Θ is the inverse function of Γ with respect to its second argument. Note that Θ is set-valued because of the property PD2 of Γ , implying that multiple values of u correspond to a given pair $\{v, \hat{f}\}$, especially if either $\hat{f} = \max \mathcal{F}$ or $\hat{f} = \min \mathcal{F}$. It is worth noting that the highest and lowest plateaus in Fig. 3(a) and Fig. 4(a) correspond to the set-valuedness of $\Theta(v, \hat{f})$. With the case of Γ illustrated in Fig. 3, $\Theta(v, \hat{f})$ can be set-valued also when $v = 0$ as can be visible as the gray rectangle areas in Fig. 3(c). In addition, Θ is not a total function, i.e., its domain is not the whole $\mathbb{R} \times \mathbb{R}$, because $\Theta(v, \hat{f}) = \emptyset$ if $\hat{f} \notin \Gamma(v, \mathcal{B}) \subseteq \mathcal{F}$.

The fact that Θ is set-valued and non-total causes inconvenience in the use of Θ in the controller. To avoid the inconvenience, it is better to prepare a total single-valued function $\Theta_s : \mathbb{R} \times \mathbb{R} \rightarrow \mathcal{B}$ that satisfies the following:

$$\Theta_s(v, \hat{f}) \in \Theta\left(v, \text{sat}_{\Gamma(v, \mathcal{B})}(\hat{f})\right), \quad \forall \hat{f} \in \mathbb{R}, \quad \forall v \in \mathbb{R}, \quad (14)$$

which means that, if $\hat{f} \in \Gamma(v, \mathcal{B})$, $\Theta_s(v, \hat{f})$ is a single-valued selection of $\Theta(v, \hat{f})$, and otherwise, $f = \Gamma(v, \Theta_s(v, \hat{f}))$ is the projection of \hat{f} onto $\Gamma(v, \mathcal{B})$ due to the property P1. In the special case where $\Gamma = \Gamma_{\text{ex}}$ in (11), one example of Θ_s can be given as follows:

$$\Theta_{s, \text{ex}}(v, \hat{f}) \triangleq \begin{cases} \text{sat}\left(Bv / (F_m - \text{sgn}(v)\hat{f})\right) & \text{if } v \neq 0 \wedge F_m - \text{sgn}(v)\hat{f} > 0 \\ \text{sgn}(v) & \text{if } v \neq 0 \wedge F_m - \text{sgn}(v)\hat{f} \leq 0 \\ 0 & \text{if } v = 0. \end{cases} \quad (15)$$

This expression can be derived by carefully examining (11) under different conditions, e.g., the sign of u and whether $|\hat{f}| < F$ or $|\hat{f}| \geq F$.

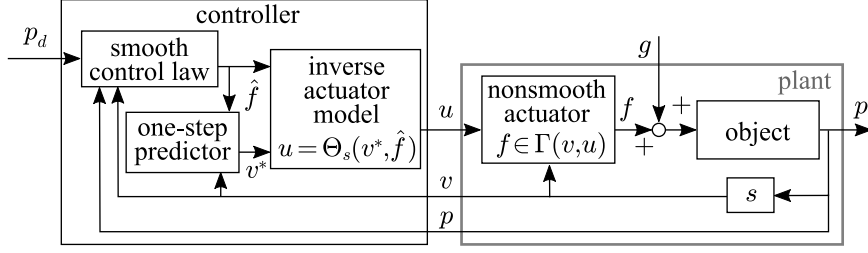


Figure 5: Implementation of a smooth controller to a nonsmooth actuator.

3.3 Implementation of a Controller

Here, one should note that the equivalence in (13) is somewhat misleading. In order to exert a non-zero force \hat{f} at the velocity $v = 0$, (13) allows for the control input $u = 0$ because $0 \in \Theta(0, \hat{f})$ for all $\hat{f} \in \mathcal{F}$, but the control input $u = 0$ at $v = 0$ obviously does not drive the actuator.

The source of the problem is that, for some velocities v , the control input u allowed by $\Theta(v, \hat{f})$ may not actually result in $f = \hat{f}$, e.g., when $v = 0$ and $\min \mathcal{F} < \hat{f} < \max \mathcal{F}$. One alternative is to attempt to realize $f = \hat{f}$ at a small time T later. That is, with a desired force \hat{f} , one can consider determining u so that

$$\hat{f} \in \Gamma(v + T(\hat{f} + g)/M, u), \quad (16)$$

or equivalently,

$$u \in \Theta(v + T(\hat{f} + g)/M, \hat{f}). \quad (17)$$

Here, $v + T(\hat{f} + g)/M$ can be viewed as a predicted velocity based on the nominal model (12a) of the plant. One may also use a single-valued function Θ_s satisfying (14) to uniquely determine u as follows:

$$u = \Theta_s(v + T(\hat{f} + g)/M, \hat{f}). \quad (18)$$

It should be noted that, if T is viewed as the sampling interval of the discrete-time device to which the controller should be implemented, (18) can be seen as a solution of the implicit (backward) Euler discretization of the plant model (12), which is

$$M(v_{k+1}^* - v_k)/T = \hat{f}_k + g_k, \quad \hat{f}_k \in \Gamma(v_{k+1}^*, u_k). \quad (19)$$

This expression is derived by substituting $\dot{v} \approx (v_{k+1}^* - v_k)/T$ to (12). Here, $k \in \mathbb{N}$ denotes the discrete-time index, v_k is the current measured velocity, and v_{k+1}^* is the velocity predicted by the plant model (12) or the velocity intended to be realized in the next timestep. We are assuming that the plant parameter M and the external force g are accurately known. The algebraic constraints in (19) can be solved as follows:

$$v_{k+1}^* := v_k + T(\hat{f}_k + g_k)/M \quad (20a)$$

$$u_k := \Theta_s(v_{k+1}^*, \hat{f}_k). \quad (20b)$$

which can be implemented as an algorithm to convert the desired actuator force \hat{f}_k to the control input u_k to the controller. To be more accurate, the control input u is to be kept constant at the value u_k for the time period $t \in [kT, (k+1)T)$. Fig. 5 illustrates this implementation scheme. It can be seen as a variant of the implicit implementation scheme [3, 7, 11, 12, 22, 27], in which the implicit discretizations of the nominal plant model and a controller are algebraically combined. It should be emphasized that the original scheme [3, 7, 11, 12, 22, 27] is to deal with a nonsmooth controller, while the scheme in Fig. 5 is to deal with a plant including a nonsmooth actuator.

One justification of using (16) and (17), with the predicted velocity $v + T(\hat{f} + g)/M$ instead of the current velocity v , is summarized as follows.

Theorem 1. *Assume that v is an absolutely continuous function of time that satisfies (12). Let \mathcal{T} be a sufficiently long time period starting from the time $t = t_0$. At the time $t = t_0$, let $v = v_0$ and $g = g_0$. Let us also assume that $g \equiv g_0$ for the period \mathcal{T} . Let $T > 0$ and $v^* = v_0 + T(\hat{f} + g_0)/M$. Then, setting $u \in \Theta(v^*, \hat{f})$ for the period \mathcal{T} results in v changing monotonically from $v = v_0$ toward $v = v^*$ until $v = v^*$ is achieved.*

A proof of Theorem 1 is given in Appendix A. It should be noted that this result also justifies the use of a non-unique selection function Θ_s in (18) and (20b) because this result does not depend on a particular choice of the value of u within the set $\Theta(v^*, \hat{f})$.

4 Implementation of Nonsmooth Controller

4.1 Controller in the Continuous-Time Domain

One important feature of the actuator (12b) is that the control input u is subject to the bound \mathcal{B} and the actuator force f is subject to a velocity-dependent bound $\Gamma(v, \mathcal{B})$. Sliding-mode control is a convenient choice for the use with bounded input because it has modes in which the control input is at its upper or lower limits [14, 15, 19]. Another beneficial aspect of sliding-mode controllers is that they allow for the design of the convergent behavior toward a desired state, through the design of the so-called sliding surface. This article considers the following controller, which is intended to be a sliding-mode controller for the plant (12):

$$u \in \text{sgn}(-\sigma) \tag{21}$$

where

$$\sigma \triangleq p + Hv - p_d. \tag{22}$$

Here, $p_d \in \mathbb{R}$ is the desired position and $H > 0$ is a positive constant representing the time constant of the convergence of p to p_d . We assume that both position p and velocity v of the plant are available to the controller, and that the desired position p_d is constant. The underlying intention of the controller (21) is to make a full effort to attract the state to the sliding mode $\sigma = 0$ when $\sigma \neq 0$. Using a time-variable p_d would not be technically difficult, but we leave it outside the scope of this paper because it would complicate the following stability analysis.

Now we show that the controller (21) can be seen as a sliding mode controller for the plant (12). The closed-loop system composed of the plant (12) and the controller (21) can be written as follows:

$$\begin{bmatrix} \dot{\sigma} \\ \dot{v} \end{bmatrix} \stackrel{\text{a.e.}}{=} \begin{bmatrix} v \\ 0 \end{bmatrix} + \begin{bmatrix} H/M \\ 1/M \end{bmatrix} (f + g) \quad (23a)$$

$$f \stackrel{\text{a.e.}}{\in} \Gamma(v, \text{sgn}(-\sigma)). \quad (23b)$$

Here, the nested set-valued functions should be read as in (10). Note that (23a) is equivalent to (12a). Because the set $\Gamma(v, \text{sgn}(-\sigma)) \subseteq \mathcal{F}$ is compact and convex for all $[\sigma, v]^T \in \mathbb{R}^2$ (due to the properties P1 and P2), the differential inclusion (23) always has a solution with respect to $[\sigma, v]^T$. (See, e.g., [26, Theorem 4.7] and the three conditions therein.) Properties of the system (23) are summarized as follows:

Theorem 2. *Consider the system (23). Let us assume that there exist $R > 0$ and $\delta > 0$ with which*

$$|g| + \delta < R < \min((-\Gamma(0, -1)) \cup \Gamma(0, 1)) \quad (24)$$

is satisfied for all $t \in \mathbb{R}_+$. (The right-hand side of (24) is positive because of the property P7 as can be seen in Fig. 3(b) and Fig. 4(b)). Then, a subset of the subspace $\mathcal{S} \triangleq \{[\sigma, v]^T \mid \sigma = 0\}$ is finite-time stable and positively invariant, and the origin $[\sigma, v]^T = 0$ is asymptotically stable. In addition, the origin is globally asymptotically stable if $g \equiv 0$.

A proof is presented in Appendix B. This result means that the controller (21) can be seen as a sliding-mode controller with the switching surface \mathcal{S} , which makes the position p exponentially converge to the desired position p_d with the time constant H under bounded disturbance g .

It should be noted that the closed-loop system (23) does not necessarily require u to be chosen as (21). It only requires f to satisfy (23) and u to satisfy (12b). That is, the satisfaction of (23) only needs the following relation:

$$u \in \Theta(v, \Gamma(v, \text{sgn}(-\sigma))) \supset \text{sgn}(-\sigma). \quad (25)$$

This means that, when $\sigma < 0$ for example, u does not have to be +1 but can be a smaller value satisfying $\Gamma(v, u) = \Gamma(v, 1)$. In this sense, one may consider (23b), as opposed to (21), to be a controller. Although it possesses a nested set-valued structure, it is a consequence of the nonsmooth actuator. It may be seen in contrast to Miranda-Villatoro et al.'s [22] controller, which is designed on purpose to possess a nested set-valued structure.

4.2 Proposed Implementation Scheme

Now, we construct a discrete-time controller algorithm to realize the closed-loop system (23), with which the switching surface \mathcal{S} in Theorem 2 is finite-time stable and the origin is asymptotically stable. Our approach presented here is to calculate the desired actuator force \hat{f} from the closed-loop system (23) through the original implicit implementation scheme [3, 7, 11, 12, 22, 27] and to use \hat{f} to obtain the control input u through the algorithm (12b) in Section 3.3.

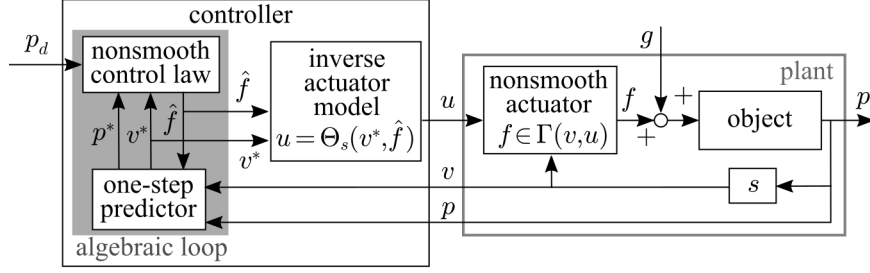


Figure 6: Proposed scheme: implicit implementation of a nonsmooth controller to a nonsmooth actuator.

First, let us apply the original implicit implementation scheme [3, 7, 11, 12, 22, 27] to the system (23) to determine the desired actuator force \hat{f} that realizes the closed-loop system (23). Let us assume that the actuator force f perfectly realizes its desired value \hat{f} and that the external force g is exactly known. Then, considering the equivalence between (23a) and (12), an implicit Euler discretization of the system (23) can be written as follows:

$$M(v_{k+1}^* - v_k)/T = \hat{f}_k + g_k \quad (26a)$$

$$p_{k+1}^* = p_k + T v_{k+1}^* \quad (26b)$$

$$\hat{f}_k \in \Gamma(v_{k+1}^*, \text{sgn}(p_{d,k} - p_{k+1}^* - H v_{k+1}^*)). \quad (26c)$$

Eliminating v_{k+1}^* and p_{k+1}^* from (26c) by using (26a) and (26b) yields the following:

$$\hat{f}_k \in \Gamma(v_{f,k} + \eta \hat{f}_k, \text{sgn}(v_{s,k} - v_{f,k} - \eta \hat{f}_k)) \quad (27)$$

where

$$v_{f,k} \triangleq v_k + \eta g_k \quad (28a)$$

$$v_{s,k} \triangleq (p_{d,k} - p_k)/(H + T) \quad (28b)$$

$$\eta \triangleq T/M. \quad (28c)$$

Possible interpretations for the intermediate variables $v_{f,k}$ and $v_{s,k}$ are that $v_{f,k}$ is the velocity that would be achieved if the actuator force \hat{f}_k was equal to zero, and that $v_{s,k}$ is the velocity that would be achieved in the ideal sliding motion if the actuator force was unbounded.

In order to solve (27) with respect to \hat{f}_k , we define a single-valued function $\Gamma_\eta : \mathbb{R} \times \mathcal{B} \rightarrow \mathcal{F}$ that satisfies the following relation:

$$f = \Gamma_\eta(v, u) \iff f \in \Gamma(v + \eta f, u). \quad (29)$$

The uniqueness of the single-valued function Γ_η satisfying (29) is given as follows:

Theorem 3. *The function Γ_η defined by (29) is a total, single-valued function of v and u .*

Proof. For any $v \in \mathbb{R}$ and $u \in \mathcal{B}$, there exists a unique $v_1 \in \mathbb{R}$ that satisfies $0 \in \Gamma(v_1, u) - (v_1 - v)/\eta$ because the right-hand side is unbounded and strictly monotone with respect to $-v_1$ due to the property P4. With such v_1 , one can obtain $f = (v_1 - v)/\eta$, which satisfies $f \in \Gamma(v + \eta f, u)$. \square

For example, the function Γ_η for the function Γ_{ex} defined in (11) can be obtained as follows:

$$\Gamma_{\eta,\text{ex}}(v, u) \triangleq \text{sat}_{FB} \left(\frac{F_m u - Bv}{\eta B + |u|} \right). \quad (30)$$

This function can be derived from (11) by using Lemmas 1 and 2. For the function Γ in Fig. 3, a closed-form expression of the function Λ that satisfies $v = \Lambda(\beta, f, u) \iff \beta v + f \in \Gamma(v, u)$ has been presented in [17]. It can be easily converted into Γ_η through $\Gamma_\eta(v, u) = (\Lambda(1/\eta, -v/\eta, u) - v)/\eta$ or $\Lambda(\beta, f, u) = (\Gamma_{1/\beta}(-f/\beta, u) - f)/\beta$.

With the function Γ_η defined by (29), one can rewrite (27) as follows:

$$\hat{f}_k = \text{sat}_{\Gamma_\eta(v_{f,k}, \mathcal{B})} ((v_{s,k} - v_{f,k})/\eta) \quad (31)$$

because we have the following relations:

$$\begin{aligned} & f \in \Gamma(v_b + \eta f, \text{sgn}(v_a - \eta f)) \\ \iff & (f \in \Gamma(v_b + \eta f, \mathcal{B}) \wedge \eta f = v_a) \\ & \vee (f \in \Gamma(v_b + \eta f, 1) \wedge \eta f < v_a) \\ & \vee (f \in \Gamma(v_b + \eta f, -1) \wedge \eta f > v_a) \\ \iff & (f \in \Gamma_\eta(v_b, \mathcal{B}) \wedge f = v_a/\eta) \\ & \vee (f = \Gamma_\eta(v_b, 1) \wedge f < v_a/\eta) \\ & \vee (f = \Gamma_\eta(v_b, -1) \wedge f > v_a/\eta) \\ \iff & f = \text{sat}_{\Gamma_\eta(v_b, \mathcal{B})} (v_a/\eta) \end{aligned} \quad (32)$$

for all v_a, v_b and f . Here, the following fact is used:

$$\begin{aligned} f \in \Gamma(v + \eta f, \mathcal{B}) & \iff \exists u \in \mathcal{B} \text{ s.t. } f \in \Gamma(v + \eta f, u) \\ & \iff \exists u \in \mathcal{B} \text{ s.t. } f = \Gamma_\eta(v, u) \\ & \iff f \in \Gamma_\eta(v, \mathcal{B}). \end{aligned} \quad (33)$$

Now, the desired actuator force \hat{f}_k is obtained as (31). With this \hat{f}_k , one can apply the algorithm (20) in Section 3.3 to obtain the control input u_k to generate the actuator force \hat{f}_k . That is, combining (31) and (20) and considering (28), one can obtain an algorithm to calculate u_k as follows:

$$v_{f,k} := v_k + \eta g_k \quad (34a)$$

$$v_{s,k} := (p_{d,k} - p_k)/(H + T) \quad (34b)$$

$$\hat{f}_k := \text{sat}_{\Gamma_\eta(v_{f,k}, \mathcal{B})} ((v_{s,k} - v_{f,k})/\eta) \quad (34c)$$

$$u_k := \Theta_s(v_{f,k} + \eta \hat{f}_k, \hat{f}_k). \quad (34d)$$

Note that (34) is the controller algorithm to be executed at every timestep. Its inputs are $\{p_k, v_k, p_{d,k}, g_k\}$; the desired position $p_{d,k}$, the plant position p_k and velocity v_k , and the estimated external force g_k . The output is u_k , which is to be used as the control input u to the actuator for the period $t \in [kT, (k+1)T)$. The other variables $\{v_{f,k}, v_{s,k}, \hat{f}_k\}$ are temporary ones, which do not have to be carried over to the next timestep.

One illustration of the proposed controller (34) is presented in Fig. 6. This algorithm also uses a one-step predictor to obtain v_{k+1}^* and p_{k+1}^* . The predicted velocity v_{k+1}^* appears as $v_{f,k} + \eta \hat{f}_k$ in (34d) although the predicted position p_{k+1}^* does not explicitly appear in the algorithm. The ‘algebraic loop’ is formed between the nominal model (i.e., one-step predictor) (12a) and the nonsmooth controller (23b), as has been the case with the original implicit implementation scheme [12, 27]. The analytical solution of the algebraic loop appears in (34c). After the algebraic constraint is solved, the predicted velocity v_{k+1}^* is used as the input to the function Θ_s in (34d) to obtain the control input u_k , as is in the case discussed in Section 3.3.

4.3 Errors in Nominal Model

It should be noted that the proposed scheme heavily depends on the nominal model of the plant including the external force. This section analyzes the effect of modeling errors and unknown disturbance to the discrete-time controller (34) applied to the plant (12).

First, one can see that the real plant (12), from which p is eliminated by using $\sigma \triangleq p + Hv - p_d$, can be approximated by the following discrete-time form:

$$\begin{bmatrix} \sigma_{k+1} \\ v_{k+1} \end{bmatrix} = \begin{bmatrix} 1 & T \\ 0 & 1 \end{bmatrix} \begin{bmatrix} \sigma_k \\ v_k \end{bmatrix} + \begin{bmatrix} \eta H_t \\ \eta \end{bmatrix} (f_k + g_k) + T^2 \begin{bmatrix} \varepsilon_{\sigma, k+1} \\ \varepsilon_{v, k+1} \end{bmatrix} \quad (35a)$$

$$f_k \in \text{conv}(\Gamma(v_k, u_k) \cup \Gamma(v_{k+1}, u_k)) \quad (35b)$$

where $\eta \triangleq T/M$ and $H_t \triangleq H + T$. In the last term of the right-hand side of (35a), $T^2 \varepsilon_{\sigma, k+1}$ and $T^2 \varepsilon_{v, k+1}$ are errors induced by the discretization, which are scaled by T^2 considering the fact that the errors of the Euler discretization are generally of the order of $\mathcal{O}(T^2)$. Because the forces f and g may vary within a timestep, f_k and g_k are set as average values within the timestep k . The errors caused by this approximation are also included in $\varepsilon_{\sigma, k+1}$ and $\varepsilon_{v, k+1}$. The actuator force f_k at the timestep k cannot be determined strictly but one can assume that it resides within the range indicated in (35b). The control input u_k is assumed to be kept constant within every timestep.

Next, by carefully tracing back the derivation in Section 4.2, one can rewrite the discrete-time controller (34) in the following form:

$$\begin{bmatrix} \sigma_{k+1}^* \\ v_{k+1}^* \end{bmatrix} = \begin{bmatrix} 1 & T \\ 0 & 1 \end{bmatrix} \begin{bmatrix} \sigma_k \\ v_k \end{bmatrix} + \begin{bmatrix} \hat{\eta} H_t \\ \hat{\eta} \end{bmatrix} (\hat{f}_k + \hat{g}_k) \quad (36a)$$

$$\hat{f}_k \in \hat{\Gamma}(v_{k+1}^*, \text{sgn}(-\sigma_{k+1}^*)) \quad (36b)$$

$$\hat{f}_k \in \hat{\Gamma}(v_{k+1}^*, u_k) \quad (36c)$$

where $\hat{\eta} \triangleq T/\hat{M}$. Here, the symbols with hats are values and functions of the nominal plant model, which may differ from those in the real plant (35). It involves the set-valuedness in (36b) and (36c), but they always have unique and closed-form solutions as follows:

$$\hat{f}_k = \text{sat}_{\hat{\Gamma}_{\hat{\eta}}(\hat{v}_{f,k}, \mathcal{B})}(-\hat{\sigma}_{f,k}/(\hat{\eta} H_t)) \quad (37a)$$

$$u_k = \hat{\Theta}(\hat{v}_{f,k} + \hat{\eta} \hat{f}_k, \hat{f}_k) \quad (37b)$$

where $\hat{v}_{f,k} \triangleq v_k + \hat{\eta} \hat{g}_k$ and $\hat{\sigma}_{f,k} \triangleq \sigma_k + T v_k + \hat{\eta} H_t \hat{g}_k$.

One can see that (36), which is an implicit form the controller, involves the predicted values σ_{k+1}^* and v_{k+1}^* , and they may differ from the true values σ_{k+1} and v_{k+1} of the plant (35). The error between the predicted and the real states can be written as follows:

$$\begin{aligned} \begin{bmatrix} \tilde{\sigma}_{k+1} \\ \tilde{v}_{k+1} \end{bmatrix} &\triangleq \begin{bmatrix} \sigma_{k+1}^* \\ v_{k+1}^* \end{bmatrix} - \begin{bmatrix} \sigma_{k+1} \\ v_{k+1} \end{bmatrix} \\ &= T \begin{bmatrix} H_t \\ 1 \end{bmatrix} \tilde{a}_k - T^2 \begin{bmatrix} \varepsilon_{\sigma,k+1} \\ \varepsilon_{v,k+1} \end{bmatrix} \end{aligned} \quad (38a)$$

where

$$\tilde{a}_k \triangleq (\hat{f}_k + \hat{g}_k)/\hat{M} - (f_k + g_k)/M. \quad (38b)$$

By using this, one can write the closed-loop system in the following discrete-time form:

$$\begin{bmatrix} \sigma_{k+1} \\ v_{k+1} \end{bmatrix} = \begin{bmatrix} 1 & T \\ 0 & 1 \end{bmatrix} \begin{bmatrix} \sigma_k \\ v_k \end{bmatrix} + \begin{bmatrix} \hat{\eta}H_t \\ \hat{\eta} \end{bmatrix} (\hat{f}_k + \hat{g}_k) + \begin{bmatrix} \tilde{\sigma}_{k+1} \\ \tilde{v}_{k+1} \end{bmatrix} \quad (39a)$$

$$\hat{f}_k \in \hat{\Gamma}(v_{k+1} - \tilde{v}_{k+1}, \text{sgn}(-\sigma_{k+1} + \tilde{\sigma}_{k+1})). \quad (39b)$$

Here, $[\tilde{\sigma}_{k+1}, \tilde{v}_{k+1}]^T$ defined by (38) can be seen as the unknown disturbance. Its major factor is \tilde{a}_k defined by (38b), which depends on the error between the estimated external force \hat{g}_k and the real (unknown) external force g_k , and the modeling error between \hat{M} and M . The discrete-time system (39) has the following properties:

Theorem 4. *Consider the system (39) and assume that \hat{g}_k , \tilde{a}_k , $\varepsilon_{\sigma,k}$, and $\varepsilon_{v,k}$ are appropriately bounded, as indicated in the proof, for all $k \in \mathbb{N}$. Then, a neighborhood of a subset of the subspace $\mathcal{S} \triangleq \{[\sigma, v]^T \mid \sigma = 0\}$ is finite-time stable and positively invariant. Moreover, a neighborhood of the origin of the system (39) is asymptotically stable.*

Appendix C presents a proof of this theorem, of which the structure is very similar to that of the proof of Theorem 2 in Appendix B. Theorem 4 means that a subset of the subspace \mathcal{S} approximately acts as a sliding surface, and that the state approximately converges to the origin as long as the disturbance is appropriately bounded. The theorem implies that the proposed discrete-time algorithm (34) implemented to the plant (12) well approximates the continuous-time closed-loop system (23) as long as the prediction errors $\tilde{\sigma}_{k+1}$ and \tilde{v}_{k+1} are small enough. One can also see that, from (38), the prediction errors $\tilde{\sigma}_{k+1}$ and \tilde{v}_{k+1} depend on the unknown component of the external force and the modeling error, but are of the order of the sampling interval T .

In most applications of sliding mode techniques, the controller gains are usually set larger than the magnitude of disturbances. In contrast, our problem setting assumes that the actuator force and the control input are bounded as can be seen in (21) and (23b), and thus the presented controller does not involve a parameter that can be interpreted as a gain.

5 Numerical Examples

Some simulation results to illustrate the proposed scheme are presented. We consider the plant (12) where a mass $M = 1$ kg is driven by an actuator modeled by Γ_{ex} defined by

(11). The external force g is given as a function $g(t)$ of time. The plant dynamics (12) is realized in the simulator with the backward Euler discretization, which provides the following closed-form algorithm:

$$f_i := \Gamma_{h/M}(v_i + hg(ih)/M, u_i) \quad (40a)$$

$$v_{i+1} := v_i + h(f_i + g(ih))/M \quad (40b)$$

$$p_{i+1} := p_i + hv_{i+1}. \quad (40c)$$

Here, the subscript $i \in \mathbb{N}$ stands for the discrete-time index in the simulator, and the timestep size is set as $h = 0.0001$ s. This timestep size h is for the plant simulation, not to be confused with the sampling period T of the controller, which has been discussed in previous sections. The values of the actuator's parameters are set as $F = 50$ N, $F_m = 60$ N, and $B = 30$ Ns/m, which are the same as those in Fig. 4.

The controller is the algorithm (34) with Γ_η and Θ_s being replaced by $\Gamma_{\eta,\text{ex}}$ in (30) and $\Theta_{s,\text{ex}}$ in (15), respectively. The controller's sampling interval is set as $T = 0.01$ s unless otherwise noted, the time constant for the sliding surface is set as $H = 1$ s, and the desired position is fixed as $p_d \equiv 1$ m. Here, notice that the sampling interval T of the controller is set much larger than the timestep size h of the plant simulation. It is for approximating the discrete-time controller applied to the continuous-time plant. The functions $\Gamma_{\eta,\text{ex}}$ and $\Theta_{s,\text{ex}}$ depend on the nominal values of the plant parameters $\{M, F, F_m, B\}$ and the disturbance $g(t)$. Their values used in the controller are hereafter denoted as $\{\hat{M}, \hat{F}, \hat{F}_m, \hat{B}, \hat{g}(t)\}$, respectively. Some different parameter settings for the controller are used in the simulations.

Fig. 7 shows simulation results of ideal situations where the external force is set as $g(t) \equiv 0$ and the plant parameters are assumed to be exactly known (i.e., $\hat{M} = M$, $\hat{F} = F$, $\hat{F}_m = F_m$, $\hat{B} = B$, and $\hat{g}(t) \equiv g(t) \equiv 0$). The results with various initial states are shown. It can be seen that, from all initial states, the state (σ, v) reaches the set \mathcal{S} (defined in Theorem 2) in finite time and reaches the origin asymptotically, illustrating Theorem 2 and Theorem 4. More precisely, the subset satisfying $|v| \leq v_s \triangleq F_m H / (BH - M) = 2.11$ m/s of \mathcal{S} is reached, being consistent with the content in the proof of Theorem 2. (A simple calculus shows that the maximum v_s satisfying (52) with $R = 0$ and Γ_{ex} defined in (30) is $v_s \triangleq F_m H / (BH - M)$ when $BH > M$.)

Fig. 8 shows results with the explicit implementation ($u = \text{sgn}(-\sigma)$, i.e., (21)) and the proposed algorithm (34) with different values of the sampling interval T . It shows that the explicit implementation results in intense chattering, which would make it practically unusable. In contrast, the proposed implementation (34) produces proper convergent behavior even with a large sampling interval $T = 0.25$ s. The step-like behavior of v with the larger T well illustrates Theorem 1, which implies that v is attracted to the predicted velocity v^* within each timestep.

In simulations reported hereafter, the external force g is given as

$$g(t) = g_0(t) + \begin{cases} -80 & \text{if } t \in [2 \text{ s}, 2.2 \text{ s}] \\ 0 & \text{otherwise} \end{cases} \quad (41)$$

where

$$g_0(t) \triangleq -20 \sin(4\pi t), \quad (42)$$

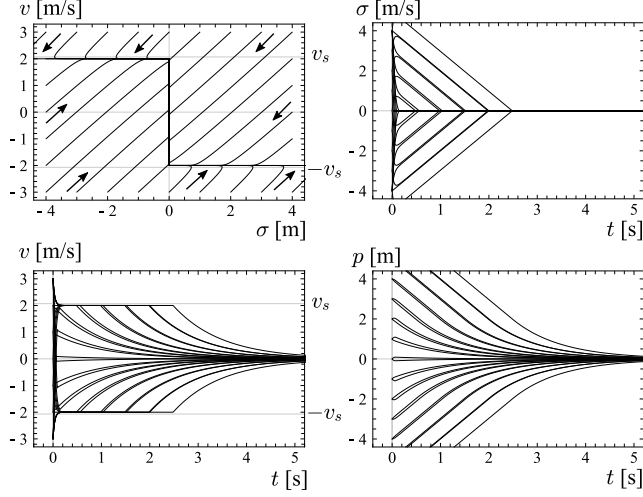


Figure 7: Simulation results of the ideal case ($\hat{M} = M$, $\hat{F} = F$, $\hat{F}_m = F_m$, $\hat{B} = B$, and $\hat{g}(t) \equiv g(t) \equiv 0$) with various initial states. The value v_s is defined as $v_s \triangleq F_m H / (BH - M) = 2.11$ m/s, which coincides with v_s appearing in Appendix B.

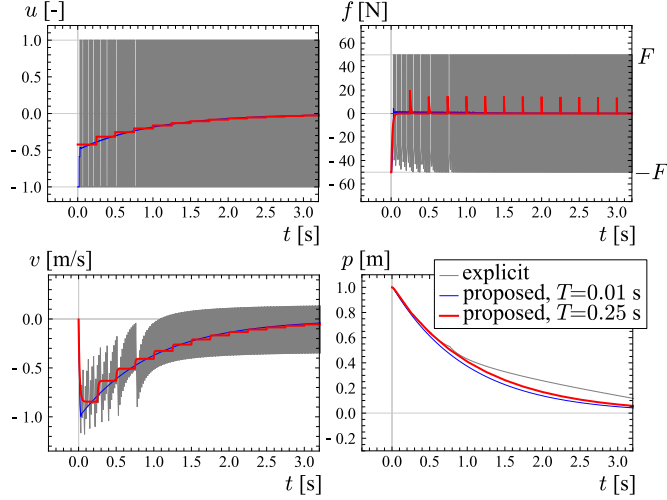


Figure 8: Simulation results of the explicit implementation ($u = \text{sgn}(-\sigma)$) and implicit implementations with $T = 0.01$ s and $T = 0.25$ s. Other settings except the initial state are the same as those of Fig. 7.

which is the sum of a sinusoidal force and an impulse-like force. Fig. 9 shows some results. The thick gray curves represent an almost ideal case, where the external force is known except the impulse-like component (i.e., $\hat{g}(t) \equiv g_0(t)$) and the plant parameters are exactly known (i.e., $\hat{M} = M$, $\hat{F} = F$, $\hat{F}_m = F_m$, and $\hat{B} = B$). The black curves represent the results of controllers whose parameter values are between -23% to $+30\%$ of the true plant parameter values. It is shown that, in all cases, the position p moves toward the target position $p_d = 1.0$ m and it actually converges after the large disturbance in $t \in [2 \text{ s}, 2.2 \text{ s}]$. The sinusoidal oscillations of the actuator force f indicate that the force f reacts to the sinusoidal disturbance g even if \hat{g} is not set to be consistent with g . It can be seen that, however, the velocity v is more influenced by the external force g when

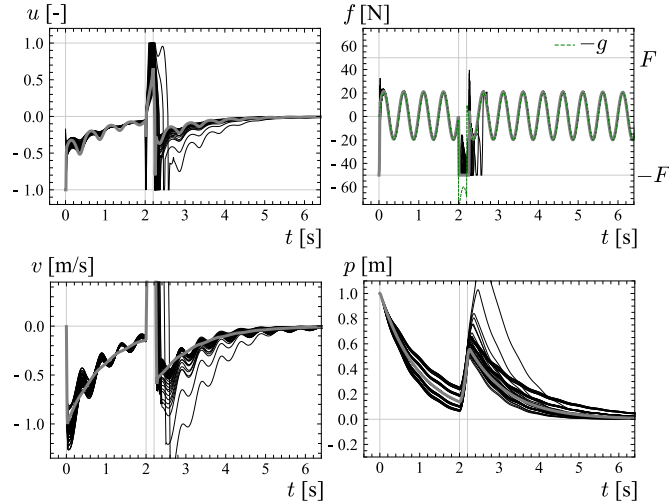


Figure 9: Simulation results with various modeling errors, in which the values of $\{\hat{M}, \hat{F}, \hat{F}_m, \hat{B}\}$ are varied between -23% to $+30\%$ of their true values $\{M, F, F_m, B\}$ of the plant. The thick gray curves represent an almost ideal case with no modeling errors and $\hat{g}(t) \equiv g_0(t)$.

$\hat{g} \neq g_0$ (the black curves) than when $\hat{g} \equiv g_0$ (the gray thick curve), although the position p eventually converges to the desired position p_d . These results exhibit a certain level of robustness of the controller against the disturbance and modeling errors.

Fig. 10 shows results with much larger \hat{M} ($= 3.0M$) and much smaller \hat{B} ($= 0.33B$). It is shown that the control input u and the actuator force f exhibit chattering although the position p converges to p_d . The parameter B is an actuator parameter that can be understood as the slope of the velocity-force curve. These results suggest that the inertia of the plant should not be overestimated and that the slope of the force-velocity curve of the actuator should not be underestimated.

In order to emulate the spool dynamics of the control valves of hydraulic actuators (see, e.g., [29]), we consider the case where the control input u generated by the controller is lagged by a low-pass filtering effect of the plant. Specifically, we consider the plant (12) with u being replaced by u_f that is determined as follows:

$$u_f = \mathcal{L}^{-1}[\mathcal{L}[u]/(\tau s + 1)^2] \quad (43)$$

where u is the input from the controller, \mathcal{L} stands for the Laplace transform, and τ is a positive constant representing the time constant of the filtering effect. Simulation results with different values of τ are shown in Fig. 11. It is shown that, although the lag in the plant affects the behavior, the position p still converges to the desired position p_d . These results suggest that the proposed controller may be applicable to hydraulic actuators with spool dynamics, while some extensions to take the lag into account would improve the performance.

6 Conclusions

This article has presented an implementation scheme of a class of nonsmooth position controllers (i.e., sliding-mode controllers) to a class of nonsmooth plants, being motivated

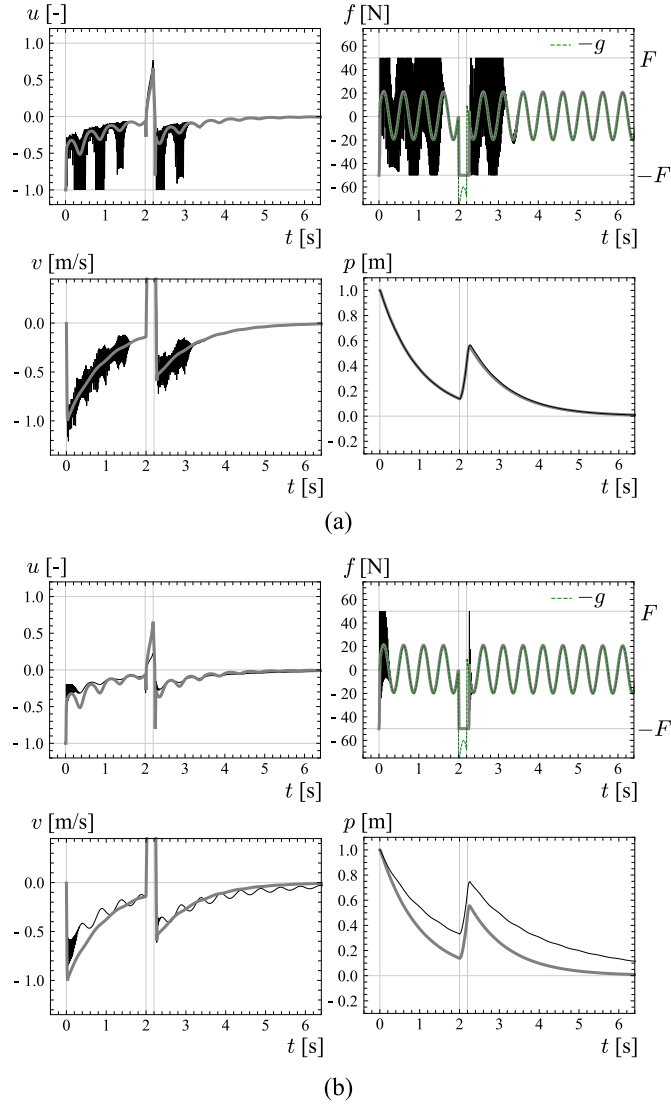


Figure 10: Simulation results with chattering caused by (a) an excessively large \hat{M} and (b) an excessively small \hat{B} . The thick gray curves represent an almost ideal case with no modeling errors and $\hat{g}(t) \equiv g_0(t)$.

by a recently-proposed quasistatic model of hydraulic actuators. The implementation is performed with the implicit discretization of the nominal plant model and the nonsmooth controller. Some stability proofs have been provided both in the continuous- and discrete-time domains. Some illustrative simulation results have also been presented.

Future improvements to the proposed controller would include the robustification of the controller against unmodeled actuator dynamics or the incorporation of the actuator dynamics model into the controller.

After the submission of this article, we have implemented an extended version of the presented controller to the swing axis of a hydraulic actuator. Some encouraging experimental results are reported in [32].

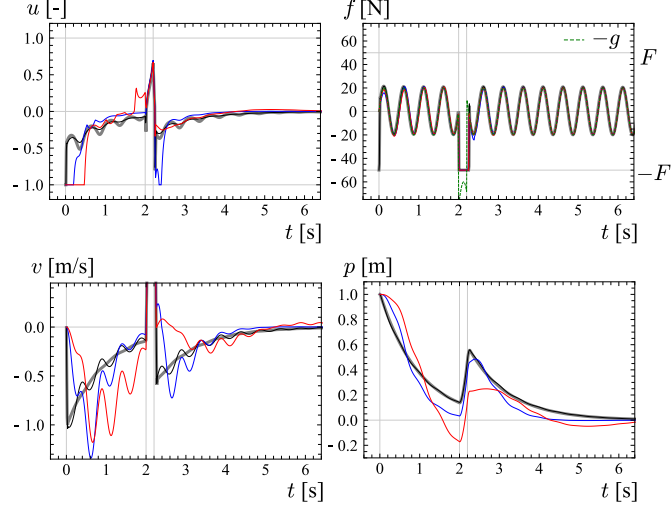


Figure 11: Simulation results with low-pass filtered inputs: $\tau = 0.4$ s (red), $\tau = 0.2$ s (blue), and $\tau = 0$ (black). The thick gray curves represent an almost ideal case with no modeling errors and $\hat{g}(t) \equiv g_0(t)$.

A Proof of Theorem 1

As a preparation for the proof of Theorem 1, we can use the following lemma:

Lemma 3. *Let $\Gamma : \mathbb{R} \times \mathcal{B} \rightrightarrows \mathbb{R}$ be a set-valued map possessing the properties P1 to P7. Then, the following statement holds true:*

$$(v_1 - v_2) (\Gamma(v_2, \Theta_s(v_1, f)) - f) \underset{\forall}{\geq} 0 \quad \forall f \in \Gamma(v_1, \mathcal{B}), \quad \forall v_1, v_2 \in \mathbb{R}. \quad (44)$$

Proof of Lemma 3. The property P4 of Γ implies that

$$(v_1 - v_2)(\Gamma(v_2, u) - f) \underset{\forall}{\geq} 0 \quad (45)$$

is satisfied for all $\{f, u, v_1, v_2\} \in \mathcal{X}_0$ where

$$\mathcal{X}_0 \triangleq \{\{f, u, v_1, v_2\} \mid f \in \Gamma(v_1, u), u \in \mathcal{B}, v_1, v_2 \in \mathbb{R}\}. \quad (46)$$

Because, using (13), $u = \Theta_s(v_1, f) \in \mathcal{B}$ implies $f \in \Gamma(v_1, u) \subseteq \Gamma(v_1, \mathcal{B})$, we have

$$\mathcal{X}_1 \triangleq \{\{f, u, v_1, v_2\} \mid u = \Theta_s(v_1, f), f \in \Gamma(v_1, \mathcal{B}), v_1, v_2 \in \mathbb{R}\} \subseteq \mathcal{X}_0. \quad (47)$$

Therefore, (45) is satisfied for all $\{f, u, v_1, v_2\} \in \mathcal{X}_1$, and it implies (44). \square

Based on this lemma, we can prove Theorem 1.

Proof of Theorem 1. For the time period \mathcal{T} , the velocity v satisfies the following:

$$M\dot{v} \stackrel{\text{a.e.}}{\in} \Gamma(v, \Theta_s(v^*, \hat{f})) + g_0, \quad v(t_0) = v_0. \quad (48)$$

Let us define $W(v - v^*) \triangleq M(v - v^*)^2/2$. Then, considering Lemma 3 and the fact that $\hat{f} + g_0 = M(v^* - v_0)/T$ by definition, we have the following:

$$\begin{aligned} \dot{W} &\stackrel{\text{a.e.}}{\in} (v - v^*) \left(\Gamma(v, \Theta(v^*, \hat{f})) + g_0 \right) \\ &= -(v^* - v) \left(\Gamma(v, \Theta(v^*, \hat{f})) - \hat{f} \right) + (\hat{f} + g_0)(v - v^*) \\ &\forall \leq -M(v_0 - v^*)(v - v^*)/T. \end{aligned} \quad (49)$$

Therefore, $\dot{W} \stackrel{\text{a.e.}}{\leq} -|v_0 - v^*|\sqrt{2M\bar{W}}/T$ is satisfied as long as $t \in \mathcal{T}$ and $v \in \text{conv}\{v_0, v^*\}$. Considering that W is an absolutely continuous function of time and that $v = v_0$ at the time instant $t = t_0$, one can see that W monotonically decreases and thus v monotonically approaches v^* until it reaches v^* in finite time. \square

B Stability Proofs: Continuous Time

Proof of Theorem 2. The proof proceeds in three steps: (a), (b), and (c).

(a) *Finite-time stability of a subset of \mathcal{S} .*

From (23), if $\sigma \neq 0$, we have the following:

$$\frac{d}{dt}|\sigma| \stackrel{\text{a.e.}}{\in} \begin{cases} \gamma_+(v, g) & \text{if } \sigma > 0 \\ \gamma_-(v, g) & \text{if } \sigma < 0 \end{cases} \quad (50)$$

where

$$\gamma_+(v, g) \triangleq (H/M)(Mv/H + \Gamma(v, -1) + g) \quad (51a)$$

$$\gamma_-(v, g) \triangleq (H/M)(-Mv/H - \Gamma(v, 1) - g). \quad (51b)$$

Here, note that $\gamma_{\pm}(v, g)$ may be set-valued because $\Gamma(v, \pm 1)$ may be set-valued as illustrated in Fig. 3.

Let us choose $v_s > 0$ so that

$$\forall v \in v_s\mathcal{B}, \quad -Mv/H + R\mathcal{B} \subset \Gamma(v, \mathcal{B}), \quad (52)$$

or equivalently,

$$\begin{aligned} \forall v \in v_s\mathcal{B}, \quad &Mv/H + R + \Gamma(v, -1) \forall \leq 0 \\ &\wedge -Mv/H + R - \Gamma(v, 1) \forall \leq 0, \end{aligned} \quad (53)$$

is satisfied. Here, recall that $\Gamma(v, \mathcal{B}) = \text{conv}(\Gamma(v, -1) \cup \Gamma(v, 1))$. The existence of v_s satisfying (52) is implied by the condition (24) (See Fig. 12(a)). With such a choice of v_s , we can see that $\gamma_{\pm}(v, g) \forall < -H\delta/M$ for all $v \in v_s\mathcal{B}$ because of (51) and (53). Therefore, $d|\sigma|/dt \stackrel{\text{a.e.}}{<} -H\delta/M$ is satisfied when $[\sigma, v]^T \in \mathcal{V} \setminus \mathcal{S}$ where

$$\mathcal{V} \triangleq \{[\sigma, v]^T \mid v \in v_s\mathcal{B}\}. \quad (54)$$

This implies that the subset $\mathcal{S} \cap \mathcal{V}$ is finite-time stable and the sliding mode at $\sigma = 0$ is established in this subset (See Fig. 12(b)).

Assume that $[\sigma, v]^T \in \mathcal{S} \cap \mathcal{V}$, $\sigma = 0$ and

$$-Mv/H - g \in \Gamma(v, \mathcal{B}) \quad (55)$$

are satisfied. In this situation, (23) implies that $f = -Mv/H - g$, which results in $\dot{\sigma} = 0$ and $\dot{v} = -v/H$. Therefore, when $[\sigma, v]^T \in \mathcal{S} \cap \mathcal{V}$, σ remains zero and $|v|$ monotonically decreases, and because $0 \in \mathcal{S} \cap \mathcal{V}$, $[\sigma, v]^T$ never deviates from $\mathcal{S} \cap \mathcal{V}$. Therefore, $\mathcal{S} \cap \mathcal{V}$ is positively invariant.

(b) *Asymptotic stability of the origin.*

Let us define a Lyapunov function candidate as follows:

$$V(\sigma, v) = \kappa|\sigma| + Hv^2/2 \quad (56)$$

where κ is a positive constant. When $\sigma = 0$ and (55) are satisfied, the system (23) is in the sliding mode, i.e., $\dot{\sigma} = 0$, and (23) results in $\dot{v} = -v/H$ and $\dot{V} = -v^2$. On the other hand, when $\sigma = 0$ is satisfied but (55) is not satisfied, $\dot{\sigma} = 0$ cannot be true and \dot{V} may not exist. Such a case may happen only at the time instants at which the state $[\sigma, v]^T$ instantaneously penetrates the surface $\sigma = 0$. Therefore, one can say that $\dot{V} = -v^2$ is satisfied for almost all t if $\sigma = 0$.

Including the case of $\sigma \neq 0$, one can see that (23) implies the following:

$$\dot{V} \stackrel{\text{a.e.}}{\in} -v^2 + \begin{cases} \gamma_+(v, g)(\kappa + v) & \text{if } \sigma > 0 \\ 0 & \text{if } \sigma = 0 \\ \gamma_-(v, g)(\kappa - v) & \text{if } \sigma < 0. \end{cases} \quad (57)$$

Recall that $\gamma_{\pm}(v, g) \vee < 0$ if $|v| \leq v_s$. Therefore, by setting $\kappa > v_s$, one can see that $[\sigma, v]^T \in \mathcal{V}$ is a sufficient condition for $\dot{V} \stackrel{\text{a.e.}}{\leq} -v^2$. When $v = 0 \wedge \sigma \neq 0$, $\dot{v} = 0$ cannot happen because of the definition (23) of the system and the condition (24). Thus, invoking LaSalle's invariance principle, one can see that the origin $(\sigma, v) = (0, 0)$ is asymptotically stable if (24) is satisfied.

Because $V(\sigma, v)$ monotonically decreases in \mathcal{V} , a subset of the region of attraction of the origin can be given as follows:

$$\mathcal{A} \triangleq \{[\sigma, v]^T \mid V(\sigma, v) \leq Hv_s^2/2\}. \quad (58)$$

Moreover, because $|\sigma|$ monotonically decreases in \mathcal{A} and it satisfies $(\mathcal{S} \cap \mathcal{V}) \subset \mathcal{A} \subset \mathcal{V}$ (see Fig. 12(b)), \mathcal{A} is also a subset of the region of attraction of the set $\mathcal{S} \cap \mathcal{V}$. From an initial state $[\sigma(0), v(0)]^T \in \mathcal{A}$, the maximum reaching time to $\mathcal{S} \cap \mathcal{V}$ is $M|\sigma(0)|/(H\delta)$ because $d|\sigma|/dt < -H\delta/M$.

(c) *Global asymptotic stability in the case of $g \equiv 0$.*

Let us set a Lyapunov function candidate as follows:

$$V_g(\sigma, v) = \max(-\kappa_p\sigma, \kappa_n\sigma) + Hv^2/2 \quad (59)$$

where κ_n and κ_p are positive constants. When $g \equiv 0$, its time derivative can be written as follows:

$$\dot{V}_g \stackrel{\text{a.e.}}{\in} \begin{cases} \gamma_{g+}(v) - \kappa_n^2 & \text{if } \sigma > 0 \\ -v^2 & \text{if } \sigma = 0 \wedge -Mv/H \in \Gamma(v, \mathcal{B}) \\ \gamma_{g-}(v) - \kappa_p^2 & \text{if } \sigma < 0 \end{cases} \quad (60)$$

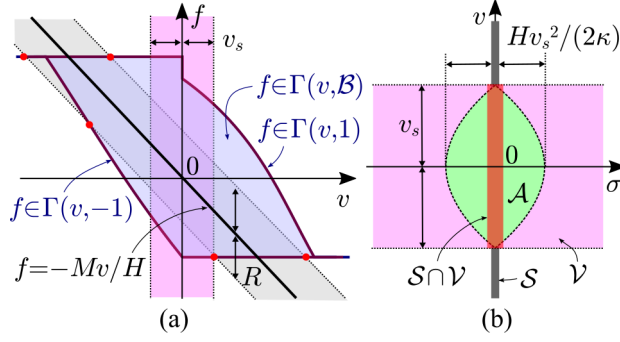


Figure 12: Illustrations for the proof of Theorem 2. (a) Γ and v_s . (b) Subsets of the state space.

where

$$\gamma_{g+}(v) \triangleq (\kappa_n + v)(\kappa_n + H\Gamma(v, -1)/M) \quad (61)$$

$$\gamma_{g-}(v) \triangleq (\kappa_p - v)(\kappa_p - H\Gamma(v, 1)/M). \quad (62)$$

The functions $\gamma_{g\pm}(v)$ can be made negative everywhere by setting κ_n and κ_p so that the following is satisfied:

$$\Gamma(-\kappa_n, -1) \ni -M\kappa_n/H, \quad \Gamma(\kappa_p, 1) \ni M\kappa_p/H. \quad (63)$$

The properties P3 and P4 of Γ imply that such κ_n and κ_p always exist and satisfy $\Gamma(0, -1) \vee \leq -M\kappa_n/H < 0 < M\kappa_p/H \leq \vee \Gamma(0, 1)$. Therefore, with the choice of κ_n and κ_p satisfying (63), (60) implies that $\dot{V}_g \stackrel{\text{a.e.}}{<} 0$ is satisfied except at the origin. Therefore, one can conclude that the origin $[\sigma, v]^T = 0$ is globally asymptotically stable if $g \equiv 0$. \square

Remark 2. *The set \mathcal{A} is a conservative estimate of the region of attraction. It does not include initial states from which the state converges to the origin after penetrating the subspace \mathcal{S} several times. A more accurate estimate of the region of attraction may be obtained by using a more complicated Lyapunov function based on the solution trajectory under the most destabilizing external force as in [15].*

C Stability Proofs: Discrete Time

Proof of Theorem 4. Let us assume that \hat{g}_k , \tilde{a}_k , $\varepsilon_{\sigma,k}$, and $\varepsilon_{v,k}$ are bounded as $|\hat{g}_k| < \hat{R} - \delta$, $|\tilde{a}_k| < U_a$, $|\varepsilon_{\sigma,k}| < U_\sigma$, and $|\varepsilon_{v,k}| < U_v$, respectively, for all $k \geq 0$, where \hat{R} , δ , U_a , U_σ , and U_v are positive constants. Let $w_{\sigma,k} \triangleq (H+T)\tilde{a}_{k-1} + T\varepsilon_{\sigma,k}$ and $w_{v,k} \triangleq \tilde{a}_{k-1} + \varepsilon_{\sigma,k} - H\varepsilon_{v,k}$. They are bounded as $|w_{\sigma,k}| < W_\sigma$ and $|w_{v,k}| < W_v$ where $W_\sigma \triangleq (H+T)U_a + TU_\sigma$ and $W_v \triangleq U_a + U_\sigma + HU_v$. Let us assume the following:

$$\hat{R} + \hat{M}W_\sigma/H < \min((-\hat{\Gamma}(0, -1)) \cup \hat{\Gamma}(0, 1)). \quad (64)$$

Let us define $x \triangleq [\sigma, v]^T$, which is the real state vector, and $x^* \triangleq [\sigma^*, v^*]^T$, which is the predicted state vector. In the following, we consider two sequences: $\{x_k\}_{k \in \mathbb{N}}$ and $\{x_k^*\}_{k \in \mathbb{N}}$. The proof proceeds in two steps: (a) and (b).

(a) *Finite-time stability of a subset of \mathcal{S} .*

From (36) and (38), one can see that the predicted states $\{x_k^*\}_{k \in \mathbb{N}}$ are recursively obtained as

$$x_{k+1}^* = \begin{bmatrix} 1 & T \\ 0 & 1 \end{bmatrix} x_k^* + \begin{bmatrix} \hat{\eta} H_t \\ \hat{\eta} \end{bmatrix} (\hat{f}_k + \hat{g}_k) + \begin{bmatrix} \tilde{\sigma}_k + T \tilde{v}_k \\ \tilde{v}_k \end{bmatrix} \quad (65a)$$

$$\hat{f}_k \in \hat{\Gamma}(v_{k+1}^*, \text{sgn}(-\sigma_{k+1}^*)) \quad (65b)$$

and that the real states $\{x_k\}_{k \in \mathbb{N}}$ are in neighborhoods of the predicted states as can be written as $x_k \in x_k^* + T\mathcal{E}$ where

$$\mathcal{E} \triangleq \left\{ \begin{bmatrix} H_t \tilde{a} - T \varepsilon_\sigma \\ \tilde{a} - T \varepsilon_v \end{bmatrix} \mid |\tilde{a}| < U_a, |\varepsilon_\sigma| < U_\sigma, |\varepsilon_v| < U_v \right\}. \quad (66)$$

Therefore, the remainder of the proof focuses on the properties of the sequence $\{x_k^*\}_{k \in \mathbb{N}}$ of the predicted states.

Equations (65) and (38) yield the following:

$$\frac{|\sigma_{k+1}^*| - |\sigma_k^*|}{T} \leq \vee \begin{cases} \gamma_+(v_{k+1}^*, \hat{g}_k, w_{\sigma,k}) & \text{if } \sigma_{k+1}^* > 0 \\ -|\sigma_k^*|/T & \text{if } \sigma_{k+1}^* = 0 \\ \gamma_-(v_{k+1}^*, \hat{g}_k, w_{\sigma,k}) & \text{if } \sigma_{k+1}^* < 0 \end{cases} \quad (67)$$

where

$$\hat{\gamma}_+(v, g, w_\sigma) \triangleq \frac{H}{\hat{M}} \left(\frac{\hat{M}v}{H} + \hat{\Gamma}(v, -1) + g + \frac{\hat{M}w_\sigma}{H} \right) \quad (68)$$

$$\hat{\gamma}_-(v, g, w_\sigma) \triangleq \frac{H}{\hat{M}} \left(-\frac{\hat{M}v}{H} - \hat{\Gamma}(v, 1) - g - \frac{\hat{M}w_\sigma}{H} \right). \quad (69)$$

Let us choose \hat{v}_s so that

$$\forall v \in \hat{v}_s \mathcal{B}, -\frac{\hat{M}v}{H} + \left(\hat{R} + \frac{\hat{M}W_\sigma}{H} \right) \mathcal{B} \subset \hat{\Gamma}(v, \mathcal{B}). \quad (70)$$

The existence of \hat{v}_s satisfying (70) is implied by the condition (64). Then, these functions satisfy $\hat{\gamma}_+(v_{k+1}^*, \hat{g}_k, w_{\sigma,k}) \leq -H\delta/\hat{M}$ and $\hat{\gamma}_-(v_{k+1}^*, \hat{g}_k, w_{\sigma,k}) \leq -H\delta/\hat{M}$ if $x_{k+1}^* \in \hat{\mathcal{V}}$ where

$$\hat{\mathcal{V}} \triangleq \{[\sigma, v]^T \mid v \in \hat{v}_s \mathcal{B}\}. \quad (71)$$

This means that $|\sigma_{k+1}^*| < |\sigma_k^*| - H\delta/\hat{M}$ is satisfied for all $\sigma_{k+1}^* \neq 0$. Therefore, the subset $\mathcal{S} \cap \hat{\mathcal{V}}$ can be reached from a neighborhood of it by the sequence $\{x_k^*\}_{k \in \mathbb{N}}$ in a finite number of timesteps. It is also the case with the subset $(\mathcal{S} \cap \hat{\mathcal{V}}) + T\mathcal{E}$ and the sequence $\{x_k\}_{k \in \mathbb{N}}$.

A careful observation on (65) and (38) shows that, if $x_{k+1}^* \in \mathcal{S} \cap \hat{\mathcal{V}}$, we have $\sigma_{k+1}^* = 0$ and

$$\frac{v_{k+1}^{*2} - v_k^{*2}}{2T} < -\frac{v_{k+1}^*}{H} (v_{k+1}^* + T w_{v,k} + \sigma_k^*/T). \quad (72)$$

This implies that, if $x_{k+1}^* \in \mathcal{S} \cap \hat{\mathcal{V}}$ and $x_k^* \in \mathcal{S}$ (i.e., $\sigma_k^* = 0$), $|v_{k+1}^*| \leq |v_k^*|$ if $|v_{k+1}^*| \geq TW_v$. Let us define

$$\mathcal{T} \triangleq \{[\sigma, v]^T \mid |v| < TW_v\} \quad (73)$$

and assume that W_v is small enough to satisfy $\mathcal{T} \subset \hat{\mathcal{V}}$. Then, one can see that, once $x^* \in \mathcal{S} \cap \hat{\mathcal{V}}$ is achieved, $\{x_k^*\}_{k \in \mathbb{N}}$ does not deviate from the subset $\mathcal{S} \cap \hat{\mathcal{V}}$ (which thus can be said to be positively invariant) and eventually reaches the terminal attractor $\mathcal{S} \cap \mathcal{T}$. It means that the real state sequence $\{x_k\}_{k \in \mathbb{N}}$ reaches $(\mathcal{S} \cap \hat{\mathcal{V}}) + T\mathcal{E}$ in finite time, stays there after that, and eventually converges to the terminal attractor $(\mathcal{S} \cap \mathcal{T}) + T\mathcal{E}$.

(b) *Asymptotic stability of the origin.*

Let us define

$$\hat{V}([\sigma, v]^T) = \kappa|\sigma| + Hv^2/2 \quad (74)$$

where κ is a positive constant. Careful derivation shows that

$$\begin{aligned} \frac{\hat{V}(x_{k+1}^*) - \hat{V}(x_k^*)}{T} &\leq_{\forall} -v_{k+1}^*(v_{k+1}^* + TW_v) \\ &+ \begin{cases} \hat{\gamma}_+(v_{k+1}^*, \hat{g}_k, w_{\sigma,k}) (\kappa + v_{k+1}^*) & \text{if } \sigma_{k+1}^* > 0 \\ 0 & \text{if } \sigma_{k+1}^* = 0 \\ \hat{\gamma}_-(v_{k+1}^*, \hat{g}_k, w_{\sigma,k}) (\kappa - v_{k+1}^*) & \text{if } \sigma_{k+1}^* < 0. \end{cases} \end{aligned} \quad (75)$$

Let us choose $\kappa > \hat{v}_s$. Then, one can see that $\hat{V}(x_{k+1}^*) < \hat{V}(x_k^*)$ if $\sigma_{k+1}^* \neq 0$ and $x_{k+1}^* \in \hat{\mathcal{V}}$ and if $\sigma_{k+1}^* = 0$ and $x_{k+1}^* \notin \mathcal{T}$. Therefore, $\hat{V}(x_k^*)$ monotonically decreases in a neighborhood of $\mathcal{S} \cap \mathcal{T}$ and thus a level set including $\mathcal{S} \cap \mathcal{T}$ is asymptotically stable in terms of the predicted state x^* . It also implies that the real state arrives in a neighborhood of a level set including $(\mathcal{S} \cap \mathcal{T}) + T\mathcal{E}$, which thus can be said to be asymptotically stable. \square

Remark 3. *The approach of the above proof is similar to that adopted in Sections V.B and V.C of [11] in that they involve the predicted states, the real states, and the error between them, and that the sliding surface is achieved by the predicted states. One feature of the above proof is that a relatively complicated Lyapunov function constructed for the continuous-time system is reused in a discretized form.*

Acknowledgment

The authors are grateful to Kobelco Construction Machinery Co., Ltd. not only for their financial support but also for motivating and encouraging us into this work. We especially thank Mr. Tomofumi Okada, Mr. Hideo Yoshihara, Mr. Takayuki Doi, Mr. Takao Nanjo, Dr. Jinjun Qiu, Mr. Koji Yamashita, and Mr. Kiyokazu Tanaka, all from Kobelco Construction Machinery Co., Ltd., for their cooperation.

References

- [1] V. Acary, O. Bonnefon, and B. Brogliato. Time-stepping numerical simulation of switched circuits within the nonsmooth dynamical systems approach. *IEEE Transactions on Computer-Aided Design of Integrated Circuits and Systems*, 29(7):1042–1055, 2010.

- [2] V. Acary and B. Brogliato. *Numerical Methods for Nonsmooth Dynamical Systems: Applications in Mechanics and Electronics*, volume 35 of *Lecture Notes in Applied and Computational Mechanics*. Springer, 2008.
- [3] V. Acary, B. Brogliato, and Y. Orlov. Chattering-free digital sliding-mode control with state observer and disturbance rejection. *IEEE Transactions on Automatic Control*, 57(5):1087–1101, 2012.
- [4] M. Al Janaideh, S. Rakheja, and C.-Y. Su. An analytical generalized Prandtl-Ishlinskii model inversion for hysteresis compensation in micropositioning control. *IEEE/ASME Transactions on Mechatronics*, 16(4):734–744, 2011.
- [5] H. H. Bauschke and P. L. Combettes. *Convex Analysis and Monotone Operator Theory in Hilbert Spaces*. Springer, 2 edition, 2016.
- [6] B. Brogliato. *Nonsmooth Mechanics: Models, Dynamics and Control*. Springer, 3rd edition, 2016.
- [7] B. Brogliato and A. Polyakov. Digital implementation of sliding-mode control via the implicit method: A tutorial. *International Journal of Robust and Nonlinear Control*, 31(9):3528–3586, 2021.
- [8] A. Cellina. On uniqueness almost everywhere for monotonic differential inclusions. *Nonlinear Analysis, Theory, Methods & Applications*, 25(9-10):899–903, 1995.
- [9] R. Changhai and S. Lining. Hysteresis and creep compensation for piezoelectric actuator in open-loop operation. *Sensors and Actuators A: Physical*, 122(1):124–130, 2005.
- [10] M. L. Corradini, G. Orland, and G. Parlang. A VSC approach for the robust stabilization of nonlinear plants with uncertain nonsmooth actuator nonlinearities — a unified framework. *IEEE Transactions on Automatic Control*, 49(5):807–813, 2004.
- [11] O. Huber, V. Acary, and B. Brogliato. Lyapunov stability and performance analysis of the implicit discrete sliding mode control. *IEEE Transactions on Automatic Control*, 61(10):3016–3030, 2016.
- [12] O. Huber, V. Acary, B. Brogliato, and F. Plestan. Implicit discrete-time twisting controller without numerical chattering: Analysis and experimental results. *Control Engineering Practice*, 46:129–141, 2016.
- [13] O. Huber, B. Brogliato, V. Acary, A. Boubakir, F. Plestan, and B. Wang. Experimental results on implicit and explicit time-discretization of equivalent control-based sliding mode control. In L. Fridman, J.-P. Barbot, and F. Plestan, editors, *Recent Trends in Sliding Mode Control*, chapter 3.2. The Institution of Engineering and Technology, 2016.
- [14] R. Kikuuwe. A sliding-mode-like position controller for admittance control with bounded actuator force. *IEEE/ASME Transactions on Mechatronics*, 19(5):1489–1500, 2014.

- [15] R. Kikuuwe. Some stability proofs on proxy-based sliding mode control. *IMA Journal of Mathematical Control and Information*, 35(4):1319–1341, 2018.
- [16] R. Kikuuwe, T. Okada, H. Yoshihara, T. Doi, T. Nanjo, and K. Yamashita. A nonsmooth quasi-static modeling approach for hydraulic actuators. *Transactions of ASME: Journal of Dynamic Systems, Measurement, and Control*, 143(12):121002, 2021.
- [17] R. Kikuuwe, T. Okada, H. Yoshihara, T. Doi, T. Nanjo, and K. Yamashita. Non-smooth quasistatic modeling of hydraulic actuators. arXiv:2102.11381, 2021.
- [18] R. Kikuuwe, N. Takesue, A. Sano, H. Mochiyama, and H. Fujimoto. Admittance and impedance representations of friction based on implicit Euler integration. *IEEE Transactions on Robotics*, 22(6):1176–1188, 2006.
- [19] R. Kikuuwe, S. Yasukouchi, H. Fujimoto, and M. Yamamoto. Proxy-based sliding mode control: A safer extension of PID position control. *IEEE Transactions on Robotics*, 26(4):670–683, 2010.
- [20] J. Kim, M. Jin, W. Choi, and J. Lee. Discrete time delay control for hydraulic excavator motion control with terminal sliding mode control. *Mechatronics*, 60:15–25, 2019.
- [21] Y.-R. Ko and T.-H. Kim. Feedforward plus feedback control of an electro-hydraulic valve system using a proportional control valve. *Actuators*, 9(2):45, 2020.
- [22] F. A. Miranda-Villatoro, F. Castaños, and B. Brogliato. Continuous and discrete-time stability of a robust set-valued nested controller. *Automatica*, 107:406–417, 2019.
- [23] M. R. Mojallizadeh, B. Brogliato, A. Polyakov, S. Selvarajan, L. Michel, F. Plestan, M. Ghanes, J.-P. Barbot, and Y. Aoustin. Discrete-time differentiators in closed-loop control systems: experiments on electro-pneumatic system and rotary inverted pendulum. hal-03125960, 2021.
- [24] S. Okishiba, R. Fukui, M. Takagi, H. Azumi, S. Warisawa, R. Togashi, H. Kitaoka, and T. Ooi. Tablet interface for direct vision teleoperation of an excavator for urban construction work. *Automation in Construction*, 102:17–26, 2019.
- [25] J. Shi, L. Quan, X. Zhang, and X. Xiong. Electro-hydraulic velocity and position control based on independent metering valve control in mobile construction equipment. *Automation in Construction*, 94:73–84, 2018.
- [26] G. V. Smirnov. *Introduction to the Theory of Differential Inclusions*. American Mathematical Society, Providence, Rhode Islands, USA, 2002.
- [27] B. Wang, B. Brogliato, V. Acary, A. Boubakir, and F. Plestan. Experimental comparisons between implicit and explicit implementations of discrete-time sliding mode controllers: Toward input and output chattering suppression. *IEEE Transactions on Control Systems Technology*, 23(5):2071–2075, 2015.

- [28] D. Wang, Z. Lijuan, H. Yu, W. Zhou, and L. Shao. Robotic excavator motion control using a nonlinear proportional-integral controller and cross-coupled pre-compensation. *Automation in Construction*, 64:1–6, 2016.
- [29] W. Wu and C. Yu. Simulation and experimental analysis of hydraulic directional control for displacement controlled system. *IEEE Access*, 6:27993–28000, 2017.
- [30] J. Xu and H.-S. Yoon. Sliding mode control of hydraulic excavator for automated grading operation. *SAE International Journal of Commercial Vehicles*, 11(2):113–123, 2018.
- [31] Y. Xu, X. Li, X. Yang, Z. Yang, L. Wu, and Q. Chen. A two-stage model for rate-dependent inverse hysteresis in reluctance actuators. *Mechanical Systems and Signal Processing*, 135:106427, 2020.
- [32] Y. Yamamoto, J. Qiu, Y. Munemasa, T. Doi, T. Nanjo, K. Yamashita, and R. Kiku-uwe. A sliding-mode set-point position controller for hydraulic excavators. *IEEE Access*, 9:153735–153749, 2021.
- [33] Y. Ye, C.-B. Yin, Y. Gong, and J.-J. Zhou. Position control of nonlinear hydraulic system using an improved PSO based PID controller. *Mechanical Systems and Signal Processing*, 83(15):241–259, 2017.
- [34] X. Zhang, S. Qiao, L. Quan, and L. Ge. Velocity and position hybrid control for excavator boom based on independent metering system. *IEEE Access*, 7:71999–72011, 2019.